Original Article

DOI: 10.5582/irdr.2024.01063

Mitochondrial metabolic maturation in postnatal right ventricle restricted by volume overload

Juan Cao[1,*], Yingying Xiao[2], Haifa Hong[2], Zhongzhong Chen[2,3,*], Wenjun Qin[2,*]

[1] Fetal Medical Center, the Affiliated Women and Children's Hospital of Ningbo University, Ningbo, China;
[2] Department of Pediatric Cardiothoracic Surgery, Shanghai Children's Hospital, School of Medicine, Shanghai Jiao Tong University, Shanghai, China;
[3] Guangzhou Women and Children's Medical Center, Guangzhou Medical University, Guangzhou, China.

SUMMARY: Right ventricular volume overload (RVVO) is a common hemodynamic abnormality in patients with congenital heart disease (CHD) and frequently leads to pathological cardiac remodeling. Our previous research demonstrated that RVVO disrupts the metabolic maturation of cardiomyocytes. Mitochondrial metabolic maturation, a crucial process in postnatal cardiomyocyte development, remains poorly understood under RVVO conditions. In this study, an mouse RVVO model was established on postnatal day 7 by creating a fistula between the abdominal aorta and inferior vena cava, confirmed by abdominal ultrasound and echocardiography. Transcriptomic analyses revealed significant downregulation of genes linked to mitochondrial metabolic maturation. Transmission electron microscopy showed impaired mitochondrial structure and maturation markers, while Seahorse assays demonstrated a marked reduction in oxidative phosphorylation rates in RVVO cardiomyocytes. These findings collectively indicated that RVVO restricted mitochondrial metabolic maturation in the postnatal RV. Targeting mitochondrial metabolic maturation could offer a promising therapeutic strategy to mitigate RVVO-induced pathological remodeling.

Keywords: volume overload, right ventricle, mitochondrial metabolic maturation, RNA sequencing

1. Introduction

Congenital heart disease (CHD) is the most common birth defect in China (*1*) and is frequently associated with a variety of complications (*2*). The right ventricle (RV) exhibits remarkable adaptability in children with CHD, functioning not only as a pulmonary ventricle under normal physiological conditions but also as a critical systemic ventricle in specific conditions. For instance, in hypoplastic left heart syndrome (HLHS) or transposition of the great arteries (TGA) following atrial switch procedures, the RV assumes systemic circulation responsibilities (*3-5*). Right ventricular volume overload (RVVO) is a common hemodynamic abnormality in children associated with CHD, and it plays a key role in determining functional status and prognosis in children with CHD (*6-8*).

Multiple studies have shown that during the early postnatal development process, cardiomyocytes undergo a metabolic transition which is critical for their maturation. From postnatal day 1 (P1) to postnatal day 7 (P7), the mouse cardiomyocytes use glycolysis as their primary energy source with a strong proliferative and regenerative potential (*3,8,9*). At P7, mouse cardiomyocytes begin the maturation process including metabolic maturation, sarcomere maturation, and electrophysiology maturation. At P21, the cardiomyocytes are fully mature and use oxidative phosphorylation as the primary energy source (*3,4*). In our previous studies, we have found that the postnatal right ventricular developmental track changed by volume overload, especially the metabolic maturation was partly interrupted by VO in a young-aged mouse RVVO model (*10-12*). There was a shift from metabolic maturation to pathologic enhanced contraction. Mitochondria, as the central hub of cellular metabolism, play an essential role in supporting the energy required by the heart (*13*). Its metabolic maturation is critical particularly during postnatal development (*14,15*). Oxidative phosphorylation and the tricarboxylic acid (TCA) cycle are the key processes in mitochondrial metabolic maturation, ensuring efficient ATP production (*16,17*). Previous studies have revealed that mitochondrial dysfunction is a hallmark of pathological cardiac remodeling (*18,19*). However, the specific impacts of VO on mitochondrial metabolic maturation in postnatal RVs remain poorly understood. Thus, explaining how VO regulating the metabolic maturation of mitochondria

in postnatal RV is critical for improving the management of CHD patients with VO.

To fully understand how VO alters the processes of mitochondrial metabolic maturation in RV, in this study, a young-aged mouse RVVO model was successfully established at P7 and followed to P21 (the endpoint of cardiomyocyte maturation). We evaluated hemodynamic changes, transcriptome, mitochondrial morphology, and mitochondrial function. Our findings provide novel insights into the mechanisms through which the RVVO restricts mitochondrial metabolic maturation, potentially contributing to relieve pathological RV remodeling.

2. Materials and Methods

Data generated in this study are available from the corresponding author upon reasonable request. All of the RNA sequencing data have been deposited in the GEO database (*https://www.ncbi. nlm.nih.gov/geo*) with accession number GSE157396.

2.1. Animal experiments

C57/BL6 mice were randomized into two groups (RVVO and control) and underwent fistula surgery or sham operation at postnatal day 7 (P7). The surgical procedure was the same as previous articles (*12*). Under general anesthesia with 4% isoflurane, a midline laparotomy was made to expose the abdominal aorta (AA) and inferior vena cava (IVC). A 0.08 mm diameter needle was used to puncture the AA through into the IVC. Then, hemostatic compression was performed for 2 min and then the abdominal wall was closed. Lidocaine was delivered locally to relieve pain. All of the procedures conformed to the principles outlined in the Declaration of Helsinki and were approved by the Animal Welfare and Human Studies Committee at the Affiliated Women and Children's Hospital of Ningbo University.

2.2. Abdominal ultrasound and echocardiography

The fistula between AA and IVC (AVF) and pulmonary artery (PA) flow were analyzed with a Vevo 2100 imaging system (Visual Sonics, Toronto, Ontario, Canada). For confirmation of an AVF, the waveform in the IVC was recorded using pulse-wave mode. To further understand hemodynamic changes in RV in both groups, the mice with patent fistula or sham operation were evaluated by echocardiography to further monitor hemodynamic changes in RV. The velocity-time integral (VTI) of the pulmonary artery (PA) blood flow, PA-velocity, RV systolic pressure, and RV stroke volume (SV) were used to evaluate RV function.

2.3. RNA quantification and qualification

The RNA sample from RV free wall was extracted with a PureLink RNA Micro Scale Kit (Life Technologies, Carlsbad, California, USA). RNA purity was checked using the NanoPhotometer®spectrophotometer (IMPLEN, Westlake Village, CA, USA). RNA integrity was assessed using the RNA Nano 6000 assay kit of the Bioanalyzer 2100 system (Agilent Technologies, Santa Clara, CA, USA). Real time-polymerase chain reaction (RT-PCR) was performed using the PrimeScript reagent kit (Takara Bio, Kusatsu, Japan). Quantitative RT-PCR (qRT-PCR) was carried out using SYBR Green Power Premix Kits (Applied Biosystems, Foster City, CA, USA) according to the manufacturer's instructions. qRT-PCR was performed on a 7900 Fast Real-Time PCR System (Applied Biosystems, Foster City, CA, USA), with the following conditions: 1 cycle at 95°C for 10 s, followed by 40 cycles of 95°C for 15 s and 60°C for 60 s. The primers were obtained from Generay Biotech Co., Ltd (Shanghai, China). The relative fold change was then calculated using the Δ CT method.

2.4. Library preparation

A total amount of 1 μg RNA per sample from RV free wall was used for the RNA sample preparations. Sequencing libraries were generated using the NEBNext® UltraTM RNA Library Prep Kit for Illumina (NEB, USA). Index codes were added to attribute sequences to each sample. The mRNA was purified from total RNA using poly-T oligo-attached magnetic beads. Fragmentation was performed using divalent cations under elevated temperature in NEB Next First Strand Synthesis Reaction Buffer (5X). First-strand cDNA was synthesized using random hexamer primers and M-MuLV Reverse Transcriptase (RNase H^-). Second-strand cDNA synthesis was subsequently performed using DNA polymerase I and RNase H. Remaining overhangs were converted into blunt ends *via* exonuclease/polymerase activities. After adenylation of the 3' ends of the DNA fragments, NEBNext Adaptors with hairpin loop structures were ligated to prepare for hybridization. To select cDNA fragments of preferentially 250-300 bp in length, the library fragments were purified with the AMPure XP system (Beckman Coulter, Beverly, MA). Then 3 μL USER Enzyme (NEB, USA) was used with size-selected, adaptor-ligated cDNA at 37°C for 15 minutes followed by 5 minutes at 95°C. Then, PCR was performed with Phusion High-Fidelity DNA polymerase, Universal PCR primers, and Index (X) Primer. Finally, PCR products were purified (AMPure XP system), and library quality was assessed on an Agilent Bioanalyzer 2100 system.

2.5. Clustering and sequencing

The clustering of the index-coded samples was performed on a cBot Cluster Generation System using a

TruSeq PE Cluster Kit v3-cBot-HS (Illumina, Shanghai, China). The sequencing was performed on an Illumina Novaseq platform, and 150 bp paired-end reads were generated.

2.6. Quality control, read mapping, and quantification of gene expression levels

Raw data in fastq format were first processed through in-house Perl scripts. Reads containing adapters, reads containing poly-N, and low quality reads were removed from raw data to generate clean data (clean reads). All of the downstream analyses were based on clean, high-quality data.

Reference genome and gene model annotation files were down- loaded from the genome website directly. The index of the reference genome was built using Hisat2 v2.0.5, and paired-end clean reads were also aligned to the reference genome using Hisat2 v2.0.5. The number of reads mapped to each gene was counted by FeatureCounts v1.5.0-p3. Fragments per kilobase of transcript sequence per million base pairs sequenced (FPKM) of each gene was calculated based on the length of the gene and read counts mapped to each gene.

2.7. Differential expression analysis

Differential expression analysis was performed using the DE- Seq2 R package (1.16.1). The resulting p-values were adjusted using Benjamini and Hochberg's approach for controlling the false discovery rate. Genes with an adjusted p-value under 0.05 found by DESeq2 were considered differential expression.

2.8. GO and KEGG enrichment analysis of differentially expressed genes

Gene Ontology (GO) enrichment analysis of differentially expressed genes was implemented by the clusterProfiler R package. GO terms with corrected p-values under 0.05 were considered to be significantly enriched. The clusterProfiler R package was used to test the statistical enrichment of differentially expressed genes in KEGG pathways.

2.9. Transmission electron microscopy

Mitochondrial morphology and sarcomere alignment were determined by transmission electron microscopy (ThermoFisher Scientific, Pittsburgh, PA, USA). The RVs removed from the mice were cut into 1 mm^3 pieces, then fixed with fresh and cold 2.5% glutaraldehyde solution overnight at 4°C. The fixed samples were dehydrated, embedded in paraffin, and sectioned into 70 nm slices. The slices were scanned with JEM-1230 (80 KV) (ThermoFisher Scientific, Pittsburgh, PA, USA).

2.10. Cardiomyocyte isolation and oxygen consumption rate (OCR) measurement

Cardiomyocytes were isolated with a Langendorff perfusion system (ADInstruments, Shanghai, China) as described previously (*9*). After perfusion, only RV free wall was removed and cardiomyocytes from RV were used for OCR measurement by Seahorse Machine.

2.11. Statistical analysis

Continuous data were expressed as means ± standard deviation. Differences were tested with Student's *t*-test if the data were normally distributed; otherwise, they were tested with the rank sum test. Values of $p < 0.05$ were considered to be statistically significant. Statistical analyses were performed using SAS software version 9.2 (SAS Institute Inc., Cary, NC, USA).

3. Results

3.1. Establishment of the RVVO Model in AVF mice

To investigate the effect of volume overload (VO) on the metabolic maturation of mitochondria in the postnatal right ventricle (RV), we created arteriovenous fistulas (AVFs) in postnatal day 7 (P7) mice. As shown in Figure 1, we observed blood flow at fistula with blood flow velocity over 800 mm/s (Figure 1, A and B). And the pulsatile blood flow at the abdominal aorta showed a slower flow rate than that at the fistula (Supplemental Figure S1, *https://www.irdrjournal.com/action/getSupplementalData.php?ID=231*). In contrast, no pulsatile flow was detected at the inferior vena cava, with a flow velocity of 0 mm/s (Supplemental Figure S2, *https://www.irdrjournal.com/action/getSupplementalData.php?ID=231*).

Furthermore, the pulmonary artery (PA)-velocity and PA-velocity-time integral (VTI) were examined to confirm there was VO in RV seven days after the AVF creation. Both the PA- velocity and the PA-VTI in the RVVO group were higher than in the sham group (Figure 1C). These results confirmed that the RVVO model was successfully established.

3.2. VO Downregulates Mitochondrial Metabolic Maturation Pathways in Postnatal RV

RNA sequencing was performed on RV tissues from AVF and sham-operated mice at P21 to investigate VO-induced changes in gene expression. The results showed that there were 1,907 differentially expressed genes between AVF and sham-operated mice at P21, among which 1,022 were downregulated and 855 were upregulated in RVVO groups (Figure 2A), $n = 3$. In order

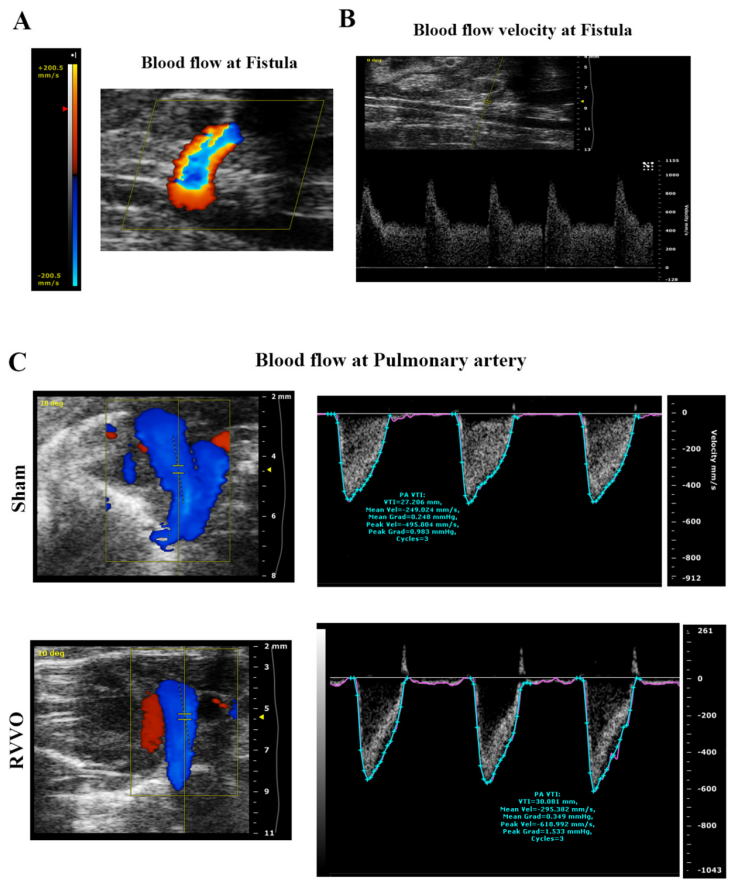

Figure 1. Construction of the abdominal aorta and inferior vena cava fistula (AVF) and verification of volume overload (VO) in the AVF group. (A) There was blood flow at fistula; **(B)** The blood flow velocity at fistula over 800 mm/s; **(C)** Representative echocardiogram of pulmonary artery (PA) velocity and velocity-time integral (VTI) in the sham and RVVO groups at P14, and the PA velocity and VTI in the RVVO group increased.

to gain a clearer understanding of the downregulation process in RVVO groups, we selected the downregulated transcripts of the RV tissues for cluster analysis. The heatmap showed that the individual mice in the same group were similar to each other but differed noticeably from the mice in the other group (Figure 2B).

Gene Ontology (GO) analysis revealed that downregulated transcripts in the RVVO group were enriched for biological processes related to energy metabolism and cellular components associated with mitochondrial structure (Figure 2C), suggesting impaired mitochondrial metabolic maturation in postnatal RV. Reactome pathway enrichment analysis further indicated that the top three downregulated pathways were mitochondrial-related (Supplemental Figure S3, *https://www.irdrjournal.com/action/getSupplementalData.php?ID=231*). To further understand the underlying mechanism by which VO modified the mitochondrial processes in postnatal RV, we applied KEGG-pathway analysis. As shown in Figure 2D, energy metabolism, oxidative phosphorylation, and citrate cycle (TCA cycle) were the most enriched terms of the KEGG pathway. This result confirmed that mitochondrial metabolic maturation was one of the most important biological processes affected by VO in postnatal RV.

3.3. Verification of RNA-seq results by examination of mitochondrial metabolic markers, morphology and respiration

To confirm that mitochondrial metabolic maturation of postnatal RV was decreased by VO, the top genes closely related to mitochondria in the gene list of RNAseq data were verified by qRT-PCR, and morphology and quantity of mitochondria were further analyzed.

As shown in Figure 3, the expression level of nine genes (Dars2, Lrpprc, Qrsl1, Mrps2, Mrpl47, Uqcc1, Gfm1, Mrps18b and Tufm), which are closely related to mitochondria, were confirmed decreased in RVVO groups, $n = 6$. Furthermore, the morphology of mitochondria was detected by transmission electron microscopy. There were fewer mitochondria in RVVO groups than in sham groups (Figure 4). In addition, the arrangement of mitochondria and sarcomeres was disordered in RVVO groups as shown in Figure 4A.

Furthermore, the effects of VO on mitochondrial respiration was analyzed by Seahorse assay. RV free wall

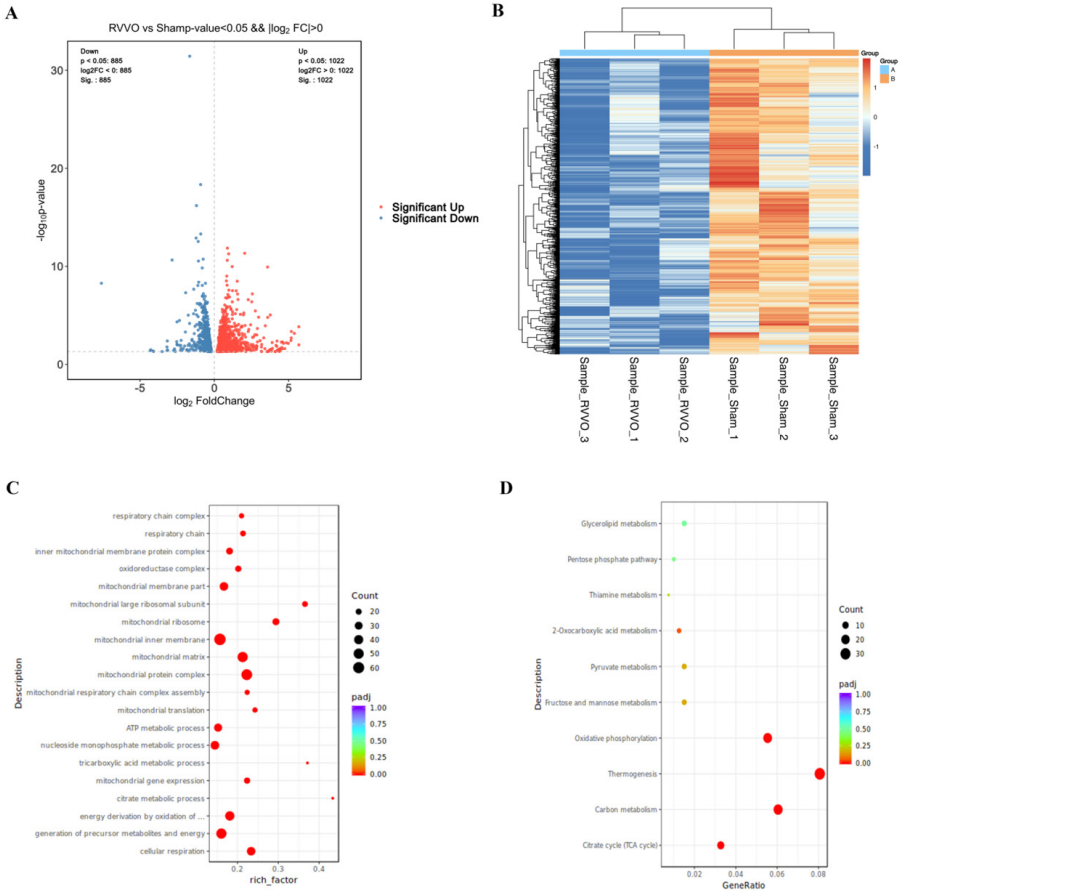

Figure 2. Transcriptome sequence revealed an enrichment of mitochondrial related genes downregulated by RVVO. (A) Volcano map of differentially expressed genes, 1022 up-regulated genes and 885 down-regulated genes in RVVO groups, $n = 3$; **(B)** The heatmap of cluster analysis of down-regulated genes (RVVO vs sham); **(C)** The top 20 GO terms of down-regulated genes were mainly related to energy metabolism and mitochondria; **(D)** The top 10 enriched terms of KEGG signaling pathways were mainly related to energy metabolism, tricarboxylic acid cycle and oxidative phosphorylation.

was removed and cardiomyocytes from RV were isolated for OCR measurement. According to the quantification of OCR levels in both RVVO and sham groups, the rate of oxidative phosphorylation was significantly decreased in RVVO group cardiomyocytes (Figure 5).

In summary, the above results confirmed that the mitochondrial metabolic maturation in postnatal RV was partly interrupted by VO.

4. Discussion

The prognosis of patients with CHDs is largely determined by RV performance, which is significantly impacted by volume overload (*6,20*). Improving our understanding of the adaption of RV to VO may help us improve our management of CHD. In our previous studies, we revealed that RVVO disrupted the metabolic maturation of cardiomyocytes. It is well known that metabolic maturation in cardiomyocytes is a hallmark of healthy cardiac development, ensuring adequate energy production to support increasing cardiac demand (*21,22*). And one of the most important processes of metabolic maturation is the change in

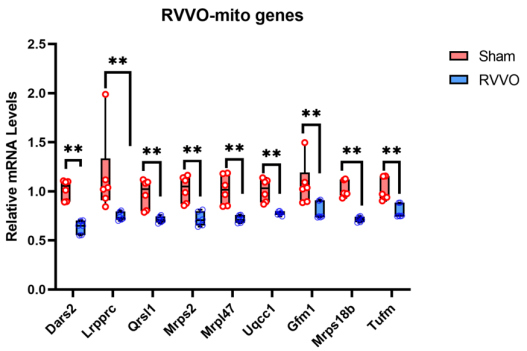

Figure 3. qRT-PCR validation of mitochondria-related genes in down-regulated gene enriched GO terms. The expression level of all mitochondria-related genes decreased in RVVO groups, $n = 6$.

mitochondria (*14,15*). However, its regulation under RVVO conditions remains poorly understood. In this study, according to our previous well-established arteriovenous fistula (AVF) model in postnatal day 7 mice (*12*), we successfully introduced RVVO groups. We also demonstrated for the first time that the impacts of VO on mitochondrial function and metabolic

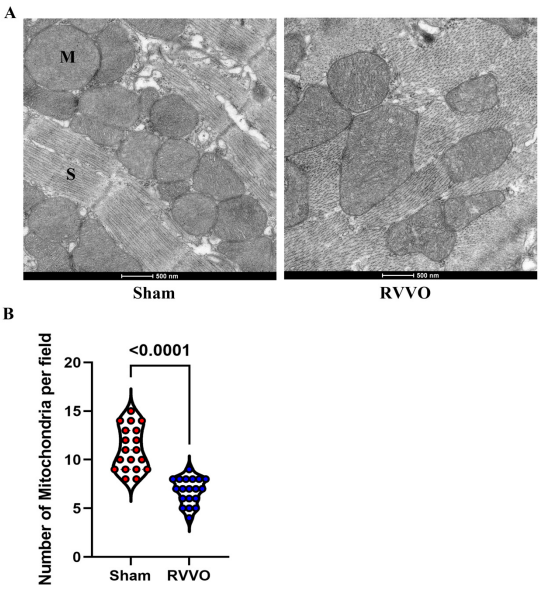

Figure 4. Transmission electron microscopy of right ventricle. **(A)** The representative images of transmission electron microscopy Of P21 RVs in sham and RVVO groups, showing that the number of mitochondria decreased and the disorder of mitochondria and sarcomeres in RVVO groups; **(B)** Quantitative analysis of mitochondria in sham and RVVO groups.

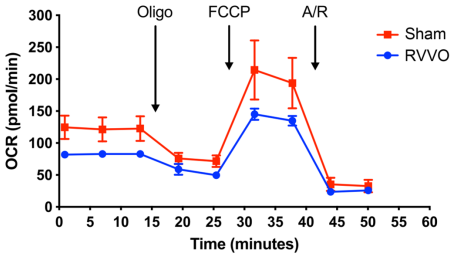

Figure 5. Quantification of OCR levels in cardiomyocytes in sham and RVVO groups. The OCR levels were decreased in RVVO group cardiomyocytes, indicating the rate of oxidative phosphorylation decreased in RVVO groups.

maturation in postnatal RVs. We observed that there was a clear shift from metabolic maturation towards pathological changes in mitochondria, characterized by reduced mitochondrial-related gene expression, deceased number of mitochondria, disordered arrangement of mitochondria and sarcomeres, and impaired oxidative phosphorylation in RVVO groups. The downregulation of mitochondrial-related genes, energy metabolism, and oxidative phosphorylation, which was indicated by transcriptomic and functional analyses, highlights the key role of mitochondrial dysfunction in this process. Furthermore, the structural abnormalities observed by transmission electron microscopy further emphasized the loss of mitochondria as a key pathological feature. These alterations not only weaken the energy efficiency of cardiomyocytes, but also may aggravate the pathological remodeling and functional decline associated with RVVO.

In summary, the current study first demonstrated that the mitochondrial metabolic maturation of cardiomyocytes in postnatal RVs was restricted by VO. This finding also provided a theoretical basis for promoting mitochondrial metabolic maturation may serve as a novel therapeutic strategy for RVVO patients. Interventions targeting mitochondrial metabolism could potentially minimize the impairments of RVVO, improving cardiac function and long-term outcomes in children with congenital heart diseases. A limitation in our study was that we only evaluated the mitochondrial metabolic maturation dysfunction in RVVO. The molecular mechanisms underlying mitochondrial dysfunction in RVVO is unknown. In the future, the molecular mechanisms and therapeutic approaches need to be explored.

Funding: This work was supported by grants from the Ningbo Top Medical and Health Research Program (No.2022020405), Key Discipline in Obstetrics (2022-B16), Ningbo science and technology project (2023Z178) and Shanghai Sailing Program (22YF1437000).

Conflict of Interest: The authors have no conflicts of interest to disclose.

References

1. Chen Z, Wang Y, Lan F, Li S, Wang J. An expanded view of infertility: The challenge of the changing profiling of major birth defects in China. Biosci Trends. 2023; 17:318-321.
2. Chen Z, Gao Y, Lu L, Li N, Liu P, Peng R, Liu L, Huang H, Fu Q, Hong H, Zhang J, Wang H. Rare loss-of-function variants reveal threshold and multifactorial inheritance of dextrocardia. Sci Bull (Beijing). 2023; 68:1993-1998.
3. Warnes CA. Transposition of the great arteries. Circulation. 2006; 114:2699-2709.
4. Broberg CS, Valente AM, Huang J, Burchill LJ, Holt J, Van Woerkom R, Powell AJ, Pantely GA, Jerosch-Herold M. Myocardial fibrosis and its relation to adverse outcome in transposition of the great arteries with a systemic right ventricle. Int J Cardiol. 2018; 271:60-65.
5. Borrelli N, Di Salvo G, Sabatino J, Ibrahim A, Avesani M, Sirico D, Josen M, Penco M, Fraisse A, Michielon G. Serial changes in longitudinal strain are associated with outcome in children with hypoplastic left heart syndrome. Int J Cardiol. 2020; 317:56-62.
6. Egbe AC, Najam M, Banala K, Vojjinni R, Faizan F, Ammash NM, Khalil F, Mathew J, Angirekula M, Connolly HM. Usefulness of right ventricular volumetric and afterload indices for risk stratification in patients with tetralogy of fallot. Am J Cardiol. 2019; 124:1293-1297.
7. Houck CA, Lanters EAH, Heida A, Taverne YJHJ, van de Woestijne PC, Knops P, Roos-Serote MC, Roos-Hesselink JW, Bogers AJJC, de Groot NMS. Distribution of conduction disorders in patients with congenital heart disease and right atrial volume overload. JACC Clin Electrophysiol. 2020; 6:537-548.
8. Fogel MA, Rychik J. Right ventricular function in congenital heart disease: Pressure and volume overload

lesions. Prog Cardiovasc Dis. 1998; 40:343-56.
9. Li H, Liu C, Bao M, Liu W, Nie Y, Lian H, Hu S. Optimized Langendorff perfusion system for cardiomyocyte isolation in adult mouse heart. J Cell Mol Med. 2020; 24:14619-14625.
10. Sun S, Hu Y, Xiao Y, Wang S, Jiang C, Liu J, Zhang H, Hong H, Li F, Ye L. Postnatal right ventricular developmental track changed by volume overload. J Am Heart Assoc. 2021; 10:e020854.
11. Wang S, Jiang C, Zhao L, Sun S, Xiao Y, Ye L, Sun Q, Li J. Metabolic maturation during postnatal right ventricular development switches to heart-contraction regulation due to volume overload. J Cardiol. 2022; 79:110-120.
12. Zhou C, Sun S, Hu M, Xiao Y, Yu X, Ye L, Qiu L. Downregulated developmental processes in the postnatal right ventricle under the influence of a volume overload. Cell Death Discov. 2021; 7:208.
13. Yu E, Mercer J, Bennett M. Mitochondria in vascular disease. Cardiovasc Res. 2012; 95:173-182.
14. Li A, Gao M, Jiang W, Qin Y, Gong G. Mitochondrial dynamics in adult cardiomyocytes and heart diseases. Front Cell Dev Biol. 2020; 8:584800.
15. Guo Y, Cao Y, Jardin BD, Sethi I, Ma Q, Moghadaszadeh B, Troiano EC, Mazumdar N, Trembley MA, Small EM, Yuan GC, Beggs AH, Pu WT. Sarcomeres regulate murine cardiomyocyte maturation through MRTF-SRF signaling. Proc Natl Acad Sci U S A. 2021; 118:e2008861118.
16. Su X, Jin Y, Shen Y, Kim IM, Weintraub NL, Tang Y. RNAase III-type enzyme dicer regulates mitochondrial fatty acid oxidative metabolism in cardiac mesenchymal stem cells. Int J Mol Sci. 2019; 20:5554.
17. Venkatesh S, Baljinnyam E, Tong M, Kashihara T, Yan L, Liu T, Li H, Xie LH, Nakamura M, Oka SI, Suzuki CK, Fraidenraich D, Sadoshima J. Proteomic analysis of mitochondrial biogenesis in cardiomyocytes differentiated from human induced pluripotent stem cells. Am J Physiol Regul Integr Comp Physiol. 2021; 320:R547-R562.
18. Piquereau J, Novotova M, Fortin D, Garnier A, Ventura-Clapier R, Veksler V, Joubert F. Postnatal development of mouse heart: Formation of energetic microdomains. J Physiol. 2010; 588:2443-2454.
19. Papanicolaou KN, Kikuchi R, Ngoh GA, Coughlan KA, Dominguez I, Stanley WC, Walsh K. Mitofusins 1 and 2 are essential for postnatal metabolic remodeling in heart. Circ Res. 2012; 111:1012-1026.
20. Rommel KP, Besler C, Noack T, Blazek S, von Roeder M, Fengler K, Ender J, Gutberlet M, Desch S, Borger MA, Thiele H, Lurz P. Physiological and clinical consequences of right ventricular volume overload reduction after transcatheter treatment for tricuspid regurgitation. JACC Cardiovasc Interv. 2019; 12:1423-1434.
21. Murphy SA, Miyamoto M, Kervadec A, *et al.*, PGC1/PPAR drive cardiomyocyte maturation at single cell level *via* YAP1 and SF3B2. Nat Commun. 2021; 12:1648.
22. Garbern JC, Lee RT. Mitochondria and metabolic transitions in cardiomyocytes: lessons from development for stem cell-derived cardiomyocytes. Stem Cell Res Ther. 2021 Mar 12; 12(1):177.

Received November 20, 2024; Revised November 29, 2024; Accepted December 6, 2024.

**Address correspondence to:*
Juan Cao, Fetal Medical Center, the Affiliated Women and Children's Hospital of Ningbo University, Ningbo, China.
E-mail: xiaojun502@vip.sina.com

Zhongzhong Chen and Wenjun Qin, Department of Pediatric Cardiothoracic Surgery, Shanghai Children's Hospital, School of Medicine, Shanghai Jiao Tong University, Shanghai, China.
E-mail: zhongzhongchen@gmail.com (ZC), qwj0130@163.com (WQ)

Released online in J-STAGE as advance publication December 13, 2024.